

Foreign Body Response Investigated With an Implanted Biosensor by *In Situ* Electrical Impedance Spectroscopy

Floyd B. Karp, Neil A. Bernotski, *Member, IEEE*, Thelma I. Valdes, Karl F. Böhringer, *Senior Member, IEEE*, and Buddy D. Ratner

Abstract—One of the principal challenges for the long-term implantation of biosensors is that the normal physiological response of the body creates a fibrotic capsule of scar tissue surrounding the implanted sensor (the foreign body response). This dense, collagenous capsule isolates the device from the local environment, causing a time-dependent degradation of the signal. We utilize this degradation or change to an electrical signal as an indicator of the physiological responses to the implantation of the biomaterial device. We thus track the foreign body response electronically, an important analytical method for our program that aims to reduce the foreign body response. We applied electrical impedance spectroscopy (EIS) to track changes of the electrical signal behavior over time between micro-electrode arrays. We have performed experiments both *in vitro* and *ex ova*. *In vitro*, we used a reservoir of phosphate buffered saline into which selected proteins were introduced that adsorb onto the electrode surface. Three proteins were studied and each was found to affect the EIS results differently. We have investigated the foreign body response *ex ova* using the chick chorio-allantoic membrane (CAM) model. Following implantation of the electrode array the chick CAM exhibited a response similar to the mammalian foreign body response. We report that the electrical signal degrades with tissue growth during the healing and remodeling following the traumatic implantation of the electrode needle through the ectoderm side of the CAM tissue.

Index Terms—Biosensor, chorio-allantoic membrane, electrical impedance spectroscopy, foreign body response, implanted medical device, wound healing.

I. INTRODUCTION

ONE OF THE principal challenges for the long-term implantation of biosensors is that the normal physiological response of the body creates a fibrotic capsule of scar tissue sur-

Manuscript received February 8, 2007; revised July 15, 2007; accepted July 20, 2007. This work was supported in part by the U.S. Department of Commerce under the National Science Foundation (NSF) Grant EEC-9529161, in part by the University of Washington Engineered Biomaterials UWEB, and in part by the NSF Engineering Research Center. The Associate Editor coordinating the review of this paper and approving it for publication was Prof. William Reichert.

F. B. Karp is with the Bioengineering Department, University of Washington, Seattle, WA 98195 USA (e-mail: floyd@u.washington.edu).

N. A. Bernotski and K. F. Böhringer are with the Electrical Engineering Department, University of Washington, Seattle, WA 98195 USA (e-mail: nbernots@u.washington.edu; karl@ee.washington.edu).

T. I. Valdes is with Becton Dickinson and Company, Franklin Lakes, NJ 07417 USA (e-mail: Thelma_Valdes@bd.com).

B. D. Ratner is with the Departments of Bioengineering and Chemical Engineering, University of Washington, Seattle, WA 98195 USA (e-mail: ratner@uweb.engr.washington.edu).

Color versions of one or more of the figures in this paper are available online at <http://ieeexplore.ieee.org>.

Digital Object Identifier 10.1109/JSEN.2007.912550

rounding the implanted sensor. This tissue acts to isolate the device from the local environment being sensed, causing a degradation of the signal. We hypothesize that this degradation or change in electrical signal character is itself an indicator of the physiological responses to the implantation of the foreign body and can be interpreted to track the progression of this response.

A. Electrical Impedance Properties of Biological Tissues

A broad historical review of the development of tissue impedance measurement methods has been compiled by McAdams and Jossinet [1]. Electrical impedance characteristics of biological materials were described in the classic chapters by Swan *et al.* [2], [3]. Grimes and Martinsen [4] and Webster [5] discuss further advanced developments in electrical impedance measurement techniques for biological tissues and provide some experimental data for comparison.

Proteins are very small compared to biological cells and extremely tiny compared to biological tissues, thus they have much less influence on biological electrical impedances than the larger mentioned structures. It is probable [4], [6] that below a threshold electrical signal frequency (about 0.5-MHz) proteins have little reactance (complex impedances). Impedance properties of various proteins do vary at frequencies above about 0.5 MHz. Proteins are large molecules with complex shapes which often have electrically charged regions at their surfaces. Because they are composed largely of carbon, oxygen, and hydrogen, the typical protein molecule is intrinsically a poor conductor of electricity. The electrical conductivity of proteins also varies because the structure of a protein can vary according to its orientation, association with other adjoining molecules, partial denaturing, and variations in internal structural conformations which affect the external charged regions.

The electrical impedance spectroscopy (EIS) method tracks the changes in magnitude and phase versus frequency between a small sinusoidal input voltage and its output measured across a medium. This method has been developed by McDonald [7] and other investigators to sense very small changes in coatings on electrodes. We have chosen to use EIS to measure the impedance changes over time in between conductive sites on an implanted micro-electrode device [8] as the wound caused by electrode implantation surgery heals. Our intention is to correlate chronological EIS data to the time-dependent physiology of wound healing. The early stages of wound healing involve thin or single layers of adsorbed proteins and migrating monocytes. These stages are followed by the formation of a growing collagen-rich fibrous capsule. The impedance variations during

these stages are very small. We chose the EIS method due to its ability to discriminate very small changes in impedance.

Other researchers are using alternate sensor methods to track wound healing and the foreign body response to implanted biomaterials *in situ*. Ho [9] *et al.* used a conductance meter to measure the electrical capacitance of skin scar tissue (wound healed) as compared to natural skin. Ho's measurements actually measured the water content of the tissues. The water content of scar tissue varies as compared to healthy tissue. Alikacem *et al.* [10] used magnetic resonance relaxometry to study tissue healing responses to coated polymer surfaces. This method cannot be used for metallic or ferromagnetic materials due to the induced currents caused by the high magnetic fields utilized.

Duan *et al.* [11] have reported that various biological structures have predictable frequency-dependent effects on electrical impedance. Fig. 1 illustrates the frequency dependence of electrical impedance in biological structures. The frequency range shown spans 0.01 Hz to 10 MHz. In the current investigation we explore the spectrum from 0.1 Hz to 100 kHz. We are most interested in the intermediate frequency range from 100 Hz to 100 kHz, which Fig. 1 indicates can be shifted up or down when electrode size changes. In particular, note that tissue response and implanted position are dominant at frequencies from 10^3 to 10^4 Hz.

Impedance measurements were carried out using a potentiostat configured to the electrodes as illustrated in Fig. 2. For the initial *in vitro* investigations the electric potential of the working micro-electrode (W) was compared with a standard calomel electrode (R). The standard calomel electrode (SCE) is a glass tube of 1-cm diameter by 5 cm long. A 1-cm² platinum mesh screen was used as the counterelectrode (C). A sterile buffered saline solution at pH 7.2 in a reservoir served as the electrolyte.

For the *in vitro* experiments with adsorbed proteins and all *ex ova* experiments an adjacent 320- μm^2 diameter iridium site (R) was utilized as a quasi-reference electrode. Iridium was chosen because it has a negligible effect on the electrical circuit between the counter and working electrodes and is charge neutral. The size and shape of the quasi-reference electrode can be configured for the desired implantation location.

Tait [6] and others have written guides for the electrical modeling and understanding of coatings on metals. The instrument arrangement shown in Fig. 2 allows evaluations and comparisons of actual electro-chemical cells.

We use the electro-chemical cell circuit model shown in Fig. 3 for our measurement. Values for the capacitive and resistive elements can be quantified from actual impedance test results. Using the mathematical software MatLab (Mathworks, Inc., Natick, MA) we can simulate the response of the circuit with the circuit element values determined from experiment. When compared, the model behavior should match the form of the actual data. These simulations are reported later in this paper.

II. MATERIALS AND METHODS

A. Sensor

We have selected micro-electrode arrays [8] as the biosensor for this investigation. These were designed for deep cortical implantation into mice or rats for the purpose of neural interface

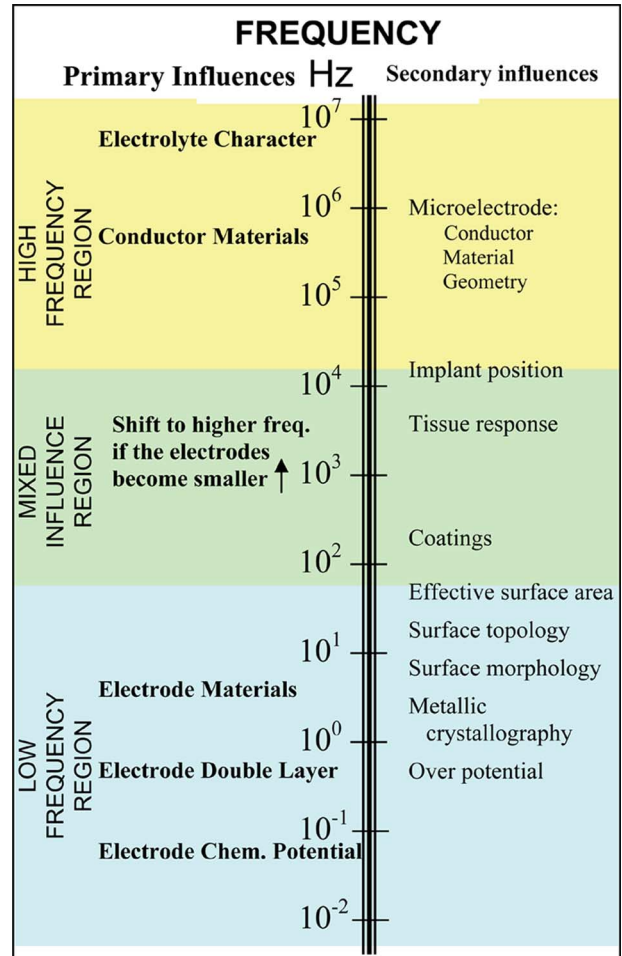


Fig. 1. Dominant effects upon electrode impedance (EI) vary with frequency. Primary and secondary factors which influence EI are shown in region of frequency where they dominate behavior of bioelectrode impedance characteristics. Modified from Duan *et al.* [11].

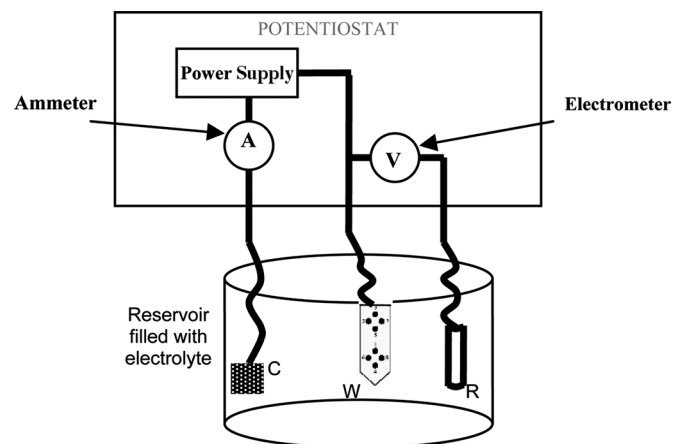


Fig. 2. Three electrode test cell schematic for EIS investigations. Note that counterelectrode (C) can be configured either as a platinum-mesh screen or as another micro-electrode site on probe tip. Note also that reference-electrode (R) can be either a standard calomel electrode or electrode site adjacent to working electrode (W).

investigations. These micro-devices were originally developed at the Center for Neural Communication Technology (CNCT)

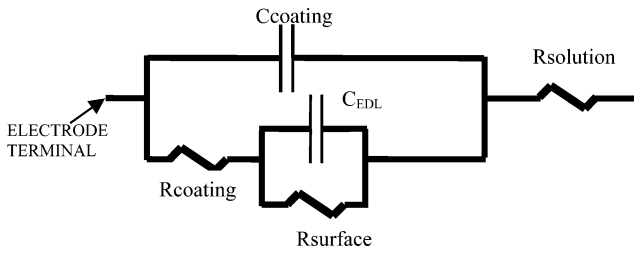


Fig. 3. General circuit model for electrode in solution with coatings (modified from Tait [6]). Two capacitive elements are shown: coating and electrical double-layer. Three resistances are shown: Faraday-surface, coating-medium, and electrolytic solution.

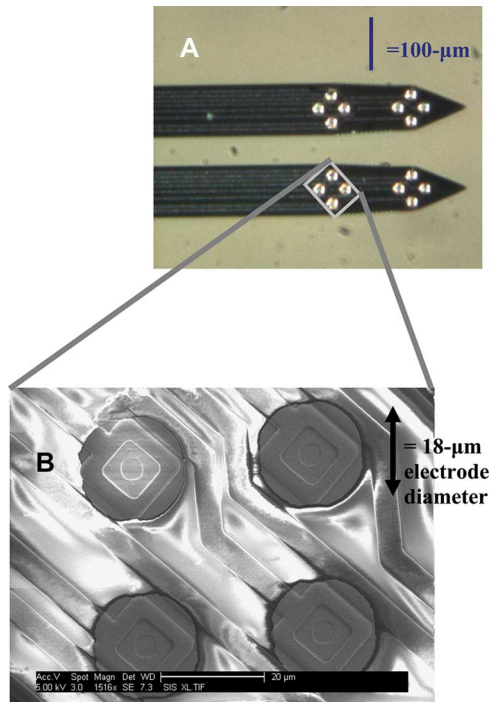


Fig. 4. Arrangement of electrodes on device surface. Lower image shows magnified details of region within box on upper image. A—optical image of device showing twin shanks each containing eight electrode sites in a double tetragonal array. B—image from scanning electron microscope showing details of four iridium-metal electrode sites and conductive traces.

(University of Michigan, Ann Arbor). The microelectrode arrays used in this project were obtained from NeuroNexus Technologies, Inc. (Ann Arbor, MI), a commercial company which fabricates the sensor devices to the specifications of the CNCT.

The micro-needle arrays are manufactured on a silicon wafer using standard microfabrication techniques. The electrodes are composed of iridium-oxide patterned onto flat $15\text{-}\mu\text{m}$ thick needles of silicon (Fig. 4). Each electrode site has a surface diameter of approximately $18\text{ }\mu\text{m}$ ($320\text{ }\mu\text{m}^2$ area). There is a distance of $35\text{ }\mu\text{m}$ between nodes. The conductive traces from each site to the outside world are composed of boron-doped silicon.

Fig. 4 shows that the electrode array is configured on twin needles. Each needle contains eight electrodes arrayed as two tetrodes. In total, there are 16 arrayed sites. The electrode metallization process yields a conformal coating of iridium on the electrode sites. Fig. 4 reveals the morphology and compositional regions of the iridium electrodes.

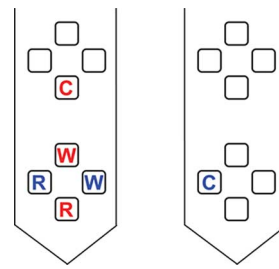


Fig. 5. Arrangement of selected electrode sites on micro-device for three electrode EIS method. Three sites may be either a horizontal row across both shanks (blue) or in vertical column (red) on a single shank. R = reference electrode, W = working electrode, C = counter electrode.

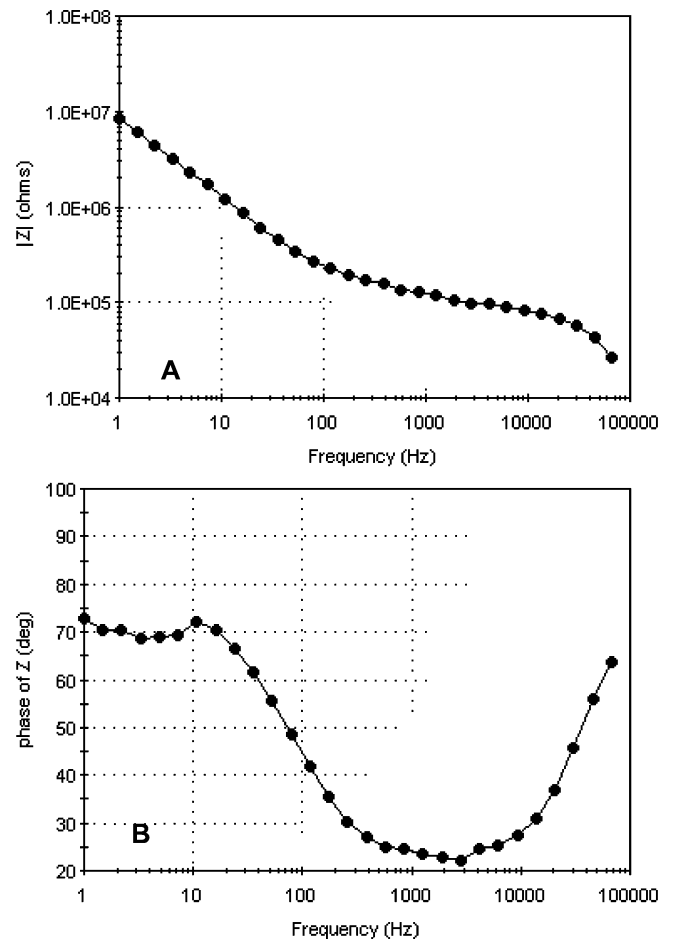


Fig. 6. EIS plots of clean electrode surfaces in 7.2-pH balanced saline reservoir. A—magnitude of impedance versus frequency. B—phase shift versus frequency.

The iridium metal surface of each electrode is activated (oxidized) prior to use. The formation of an activated surface is due to the creation of a porous, hydrated, multilayer iridium-oxide structure. This IrO_2 structure has a relatively large effective surface area for charge transfer which permits measurable saturation currents without causing electrolysis of the solution.

B. Measurement of Changes in Electrical Signal

We have applied the technique of EIS to track the changes of the electrical signal response over time as the electrode needles become encapsulated. A sinusoidal voltage was applied between the counterelectrode and working electrode while mea-



Fig. 7. Device positioned with biosensor implanted into chick chorio-allantoic membrane at day 7.

suring the resulting current between these electrodes. A third electrode provides a potential reference between the electrodes and the medium. This medium could include a salt solution and/or protein serum, biological fluid, or developing tissue. As the properties of the medium change, this is reflected in the electrical impedance spectrogram.

C. *In Vitro* Trials of Biosensor

The purpose of the saline reservoir trials was to verify that changes due to the foreign body response were detectable with EIS, specifically that the sensor and instrumentation were capable of measurements that allowed differentiation between anticipated changes in the bioelectrode environment.

Experiments were performed *in vitro* using a reservoir of phosphate buffered saline (PBS) at 7.2 pH with the controlled addition of three selected proteins. We selected collagen and fibronectin because these proteins are involved in the wound healing process. We selected egg white (mixed proteins with a major component of albumin) because in the *ex ova* model the electrodes are exposed to this protein serum. The base-line impedance spectrograph for clean electrodes in fresh PBS is shown in Fig. 6.

A PerkinElmer model 263 potentiostat (PerkinElmer Company, a division of AMETEK Princeton Applied Research, Oak Ridge, TN) was used to electrically control and measure the electrode system shown in Fig. 2. For signal measurement a Princeton Applied Research model 5210 lock-in amplifier is used. These instruments are operated by a LabView program (Texas Instruments, Dallas, TX) running on a laboratory PC computer (Dell Computers, Inc., Dallas, TX) through a general purpose interface bus (GPIB). In addition, *SineStat* software (PerkinElmer, Inc.) is used for data collection and graphical representations.

Repeated experiments were conducted with the twin needle probe surfaces coated by adsorption for 60 min with either Type-1 collagen (0.1 mg/ml), egg white (1%) or fibronectin (0.1 mg/ml) within the reservoir previously filled with saline. Five trials were carried out for each system. Between trials, probes were thoroughly cleaned with mildly agitated detergents (SDS, Tide), solvents (methyl-alcohol and hexane), and electric

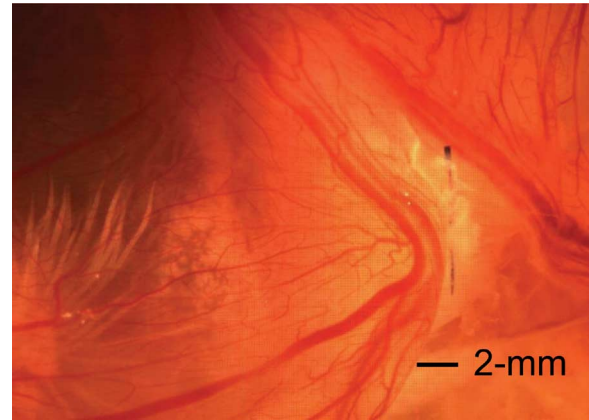


Fig. 8. Transmitted light view of material control electrode within viable *ex ova* chorio-alantoic membrane at nine days following implantation (gestation day 16). Note fibrous structure surrounding electrode shank.

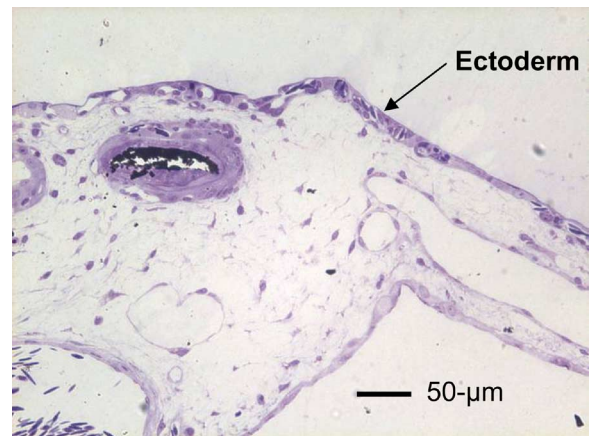


Fig. 9. Ultra-thin 0.7- μm cross-sectional slice of electrode within chorio-alantoic membrane following nine days of implantation (gestation day 16). Note fibrous structure surrounding fractured black electrode material. Stained with 1% toluidine blue.

potential methods (-2.8 V for 3 min, $+2.2$ V for 3 min). Prepared electrodes were stored in fresh deionized water (18 Mohm) to prevent dehydration of the porous iridium-oxide activated surface.

D. Circuit Model and Mathematical Simulation

For the circuit of Fig. 3, the Laplace transform of the impedance is given by (1), as shown at the bottom of the next page, where s is the complex angular frequency from the Laplace transform and

- R_{Sol} solution resistance;
- R_C coating resistance;
- C_C coating capacitance;
- R_{Surf} surface resistance;
- C_{EDL} electric double layer capacitance.

At high frequencies (large values of s), the impedance becomes R_{Sol} . If the time constant of the coating (τ_C) is much larger than the time constant of the electric double layer (τ_{EDL}),

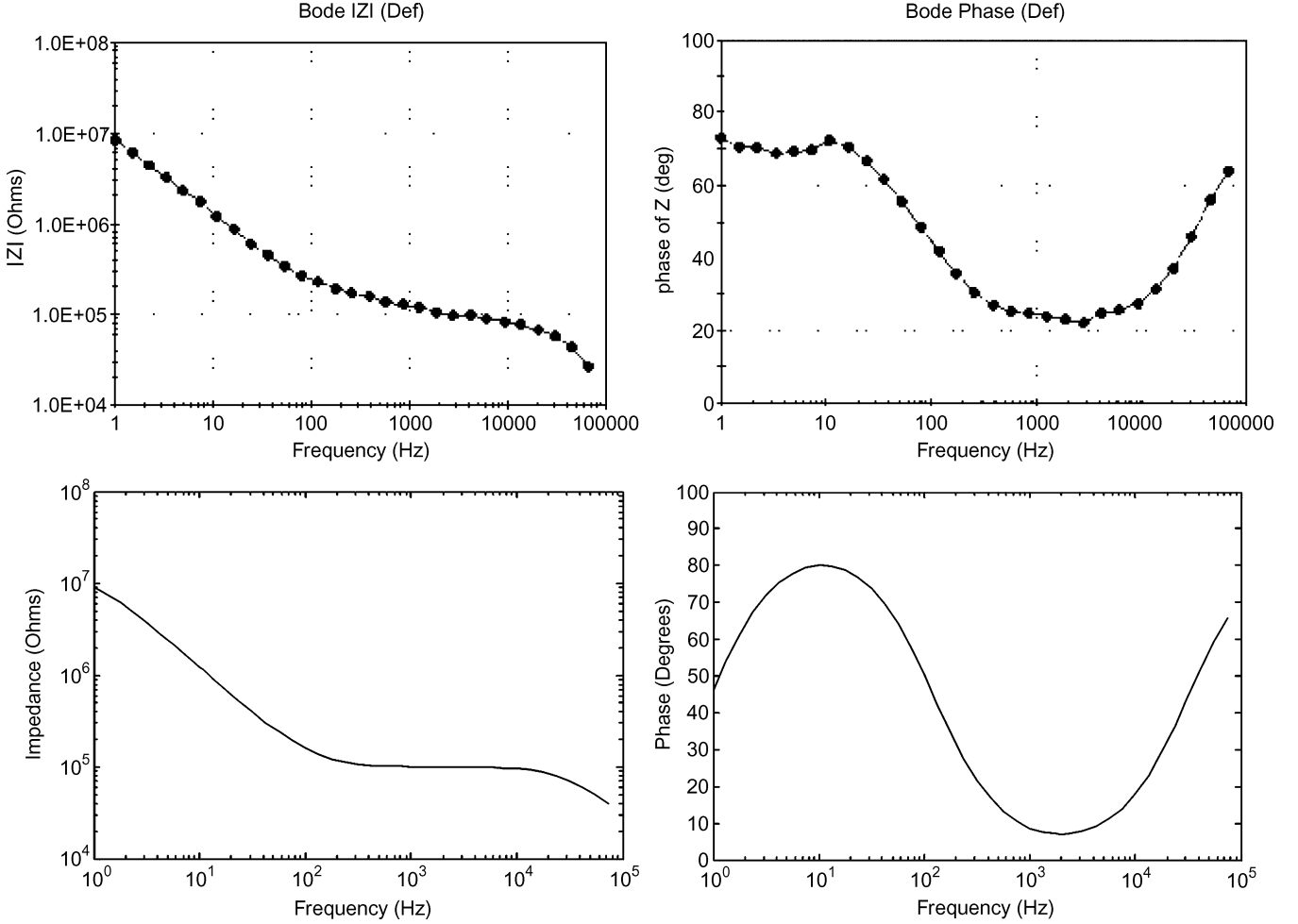


Fig. 10. Comparison of experimental data (top) and simulated data (bottom) for impedance behavior from 1 Hz to 100 kHz. Left, magnitude versus frequency. Right, phase versus frequency. Experimental data is from “clean electrode” shown in Fig. 6.

then in the frequency range around τ_{EDL}^{-1} the impedance is approximately $R_{Sol} + R_C$. This is generally the case because typically $R_C \gg R_{Sol}$ and $C_{EDL} \gg C_C$. The final resistance can be determined at low frequencies (dc), where the impedance becomes the sum of R_{Sol} , R_C , and R_{Surf} . The two capacitance values may be approximated from the frequency at which the corresponding capacitive reactance and consequently phase angle is at its peak. This occurs at radial frequencies τ_{EDL}^{-1} and τ_C^{-1} for the electric double layer and coating, respectively. Because τ_C is typically much larger than τ_{EDL} the capacitance values are approximately equal to

$$C_{EDL} = \frac{\tau_{EDL}}{R_{Surf}}, \quad C_C = \frac{\tau_C}{R_C}. \quad (2)$$

The values determined from the experimental data are reported in Section III.

E. Simplified In Vivo Model

The foreign body response was investigated using the healing process of the chick chorio-allantoic membrane (CAM) *ex ova* as the model living system. Fresh fertilized eggs (Hyline Farms, Puyallup, WA) were incubated at 39 °C for 3.5 days then cracked and emptied into clean, warm Petri dishes. These were covered and incubated for 4 days of additional gestation.

On the seventh day, under sterile conditions, the sensor device was positioned on a small stand set within a 1-l Pyrex glass warm flask. The electrode probe tip was inserted into the CAM

$$\frac{(R_{Sol}R_C C_C)s^2 + \left[R_C + R_{Sol} + \left(\frac{R_{Sol}R_C C_C + R_{Sol}R_{Surf}C_C}{R_{Surf}C_{EDL}} \right) \right] s + \left[\frac{R_{Sol} + R_C + R_{Surf}}{R_{Surf}C_{EDL}} \right]}{[R_C C_C]s^2 + \left(\frac{R_C C_C + R_{Surf}C_C + R_{Surf}C_{EDL}}{R_{Surf}C_{EDL}} \right) s + \left(\frac{1}{R_{Surf}C_{EDL}} \right)} \quad (1)$$

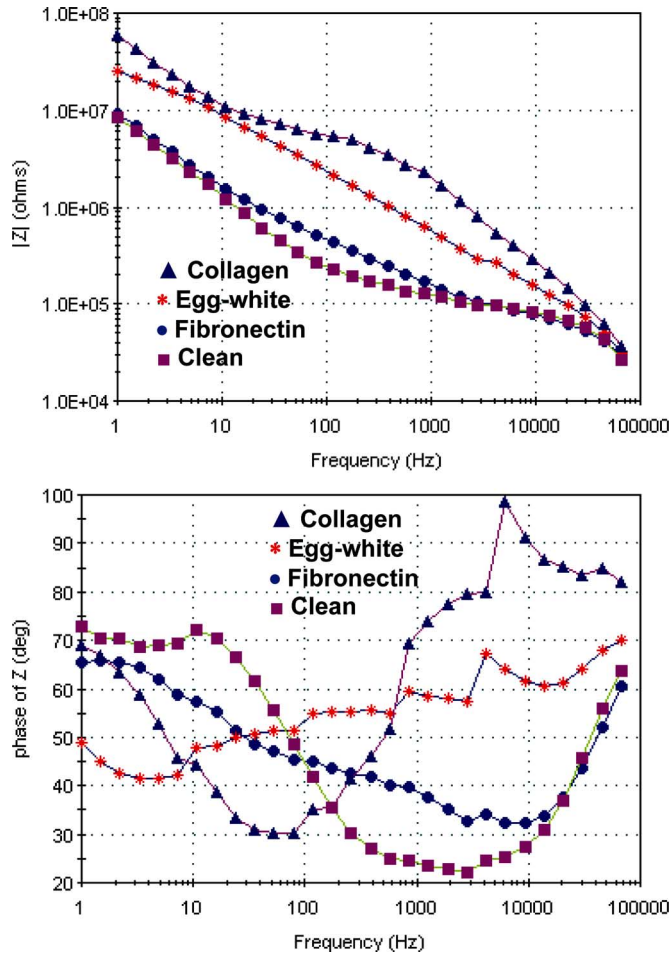


Fig. 11. EIS plots of impedance magnitude and phase between electrodes coated with: ▲ Collagen, * Egg white, ● Fibronectin, and ■ Clean.

by visual guidance with efforts to position the probe tip approximately 1.5 cm from the umbilicus–abdominal junction of the chick.

Following implantation of the electrode array probe tip, the chick CAM continues to develop. The region wounded by insertion of the probe tip begins to heal. It develops the common physiological stages closely resembling the normal mammalian foreign body response.

After implantation of the electrode probe into the CAM membrane, we performed EIS measurements periodically during the following days of further *ex ova* incubation. Gestation periods have been extended to more than 220 hours post-implantation with viable CAM and functional electrodes (>day 16).

Nonfunctional electrode probe tips were obtained for use as material controls for implantation and destructive histological comparison models. Implantation methods were identical to the methods utilized during active electrode implantation.

At day 16, histological examinations were performed on subjects with the CAM containing electrodes (Fig. 9). First, the tissues are fixed with a spray mist of 10% formalin solution. This formalin mist is effective at both rapid fixation of the ovum as well as for intermediate time tissue storage. The tissue is micro-dissected and floated off onto a urethane sponge transfer block.

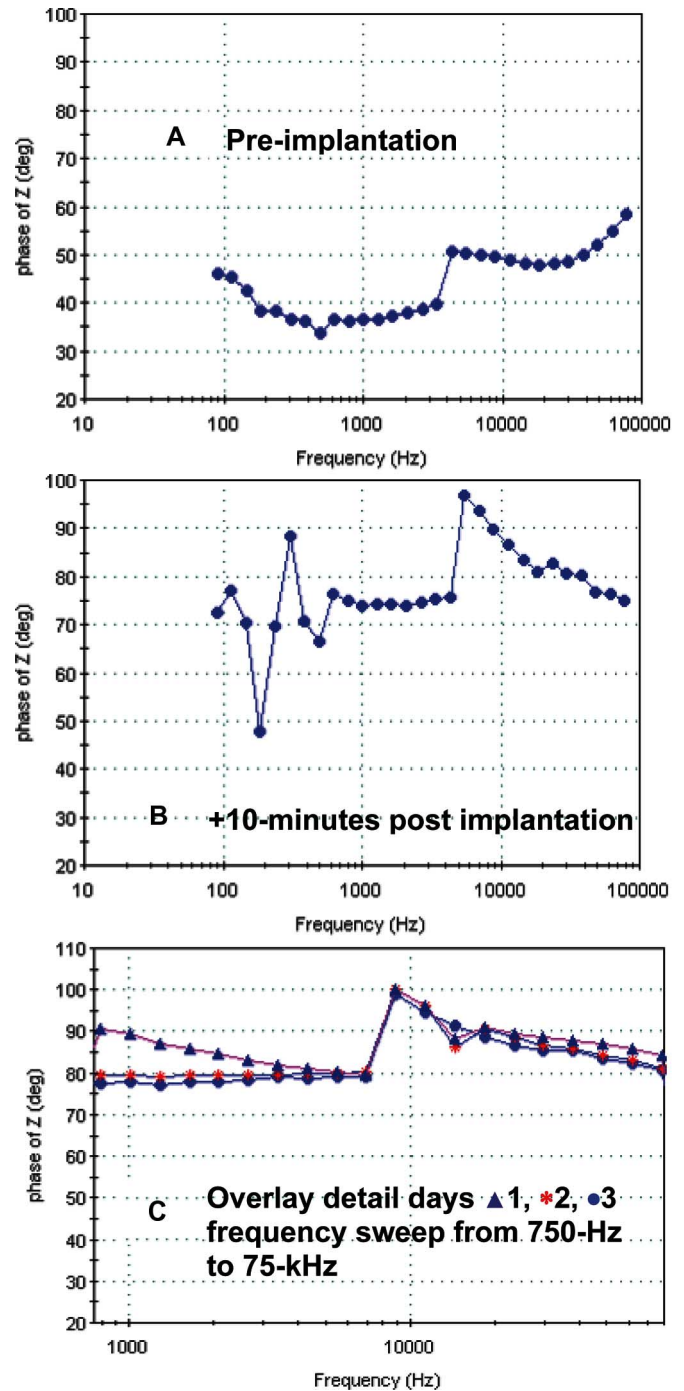


Fig. 12. Graphs in A and B show frequency spectrum from 100 Hz to 100 kHz. Graphs in C show frequency region of greatest biological interest from 750-Hz to 75 kHz.

The tissue is ethyl-alcohol dehydrated and then exchanged with xylene followed by impregnation with Epon A.2 Resin (Hexion Specialty Chemicals Company, Columbus, OH). The resin is thermally cross linked at 60 °C and becomes rigid and tough enough to permit surface shearing to 0.7- μm thickness by utilizing a diamond-edged histological preparation system. The thin sections are mounted upon glass slides and stained with 1% toluidine blue.

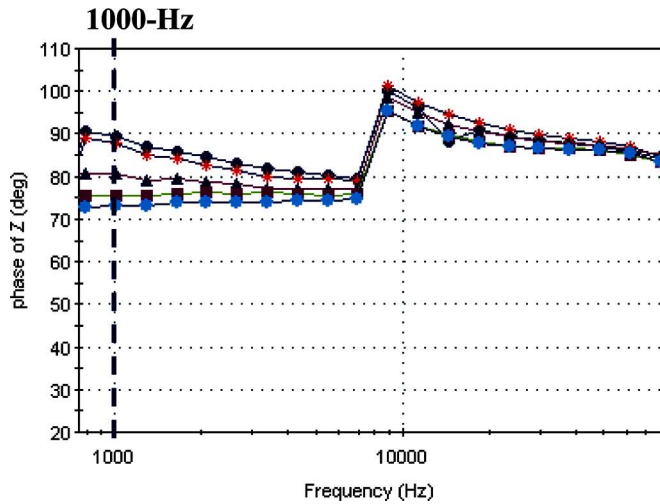
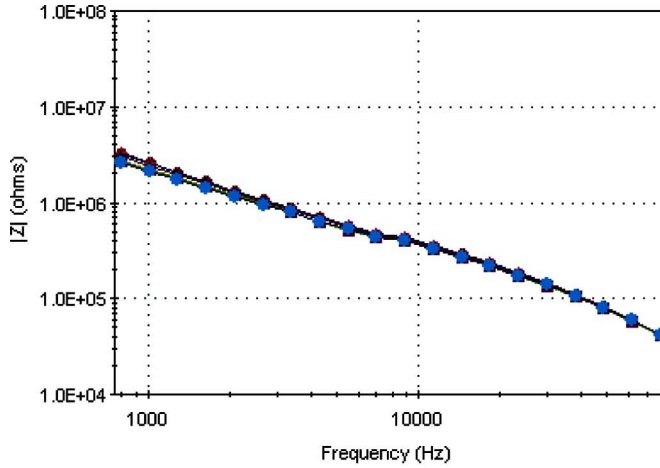


Fig. 13. Overlays of response from days •4, *5, ▲6, ■7, and ●8.

III. RESULTS AND DISCUSSION

A. Circuit Model and Mathematical Simulation

Using the method outlined in Section II-D and the experimental data shown in Fig. 6 (clean electrode), we can estimate component values for the general circuit model to be

$$R_{\text{Sol}} \approx 1 - \text{k}\Omega$$

$$R_C \approx 100 - \text{k}\Omega$$

$$C_C \approx 50 - \text{pF}$$

$$R_{\text{Surf}} \approx 13 - \text{m}\Omega$$

$$C_{\text{EDL}} \approx 13 - \text{nF}.$$

Fig. 10 shows a comparison of the experimental EIS data with the simulated output of the general circuit model using the estimated values above. The simulated output results directly from the Laplace transform equation and plots were obtained using Matlab software. The two sets of magnitude and phase plots contain differences revealing that the actual bioelectrode system is more complex than the general circuit model shown in Fig. 3. These differences may be attributed to higher order complexity in the biosensor circuit and nonlinear behavior in the actual system.

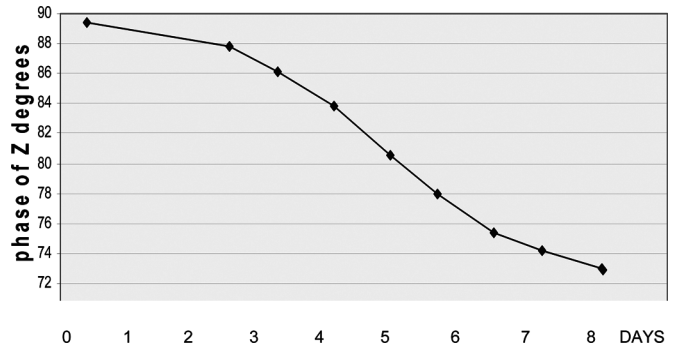


Fig. 14. Phase shift of impedance at 1000 Hz versus time.

B. Analysis of In Vitro EIS Trials

The *in vitro* EIS trials with probes coated with fibronectin, egg white, and collagen displayed distinct frequency responses as shown by the Bode plots in Fig. 11. The comparison between the three protein coated electrodes and the base-line impedance spectrograph for clean electrodes in Fig. 6 reveals different characteristic response curves. The data shown for clean and coated (3) were obtained on the same electrode device. (There are subtle EIS behavior variations between devices from the same manufacturer.)

C. Analysis of Ex Ova Healing of Chick CAM

The graphs in Fig. 12(A) and (B) show the EIS phase shift for a clean electrode and immediate post-implantation. The graph in Fig. 12(C) shows the frequency region of greatest biological interest. Greatest interest means that the frequency region (as shown in Fig. 1) has principle factors that are biologically influenced at the scale appropriate to wound healing and the foreign body response. Data from repeated implants ($n = 20$) in the chorio-allantoic membrane (CAM) of fertilized chicken eggs *ex ova* confirm that EIS behavior shows a predictably changing response of decreasing phase shift for frequencies from 750 Hz to 30 kHz (Fig. 13) during the time ($> \text{day } 3$) following the initial post-trauma period.

The graphs in Fig. 13 show that both the phase shift and impedance decline with time. We attribute this decline to an increase in the coating capacitance. For the circuit model in Fig. 3, this trend can occur when an increasing coating capacitance dominates over changes in other circuit components. This is analogous to the impedance trends reported by Grill and Mortimer [12] for time-dependent changes in resistivity during the early period of encapsulation tissue growth.

The observed impedance trend can be attributed to the increased collagen observed in the histological controls and with the observed collagen-rich structures surrounding the implanted probe needle shown in Fig. 8 (white tissues). This tissue growth occurs during the healing and remodeling of the CAM following the (relatively) traumatic implantation of the electrode needle through the ectoderm side of the tissue.

Analyzing the phase shift at a single frequency, 1 kHz, over eight days can be seen in Fig. 14.

Histological examination of samples of membrane tissues with implanted probe tips confirmed that the chick CAM wound healing processes adjacent to the implanted probe are similar

to the mammalian foreign body response. The CAM tissues showed ectoderm hyperplasia and had monocyte activation with giant cell formation adjacent to the implanted probe tip. A collagen-rich extra cellular matrix was observed in 0.7- μm sections stained with 1% toluidine blue.

D. Future Work

Future *ex ova* experiments will include utilizing the four-electrode impedance measuring method first developed by Schlumberger. Also, we will quantify the amount of each protein per unit area coating the electrode surfaces so that the importance of both protein type and total protein level can be assessed. In addition, experiments are planned where the electrode array will be coated with substances such as tetraglyme or dexamethasone which are believed to alter the foreign body response. We will compare the electrical signal sensitivity behavior of the coated electrodes to uncoated electrodes.

Upon completion of these *ex ova* experiments, we will track *in vivo* electrical signal changes by placing the electrode array within the subcutaneous musculature tissue of a small rodent animal model which also allows a longer duration of study. The initial pilot study *in vivo* trials of the biosensor using a Sprague-Dawley rat for subcutaneous intramuscular implantation of the electrode array are currently underway.

E. Conclusion

We have demonstrated that an implantable array of micro-electrodes can be utilized as a biosensor to distinguish the change in its environment caused by the growth of a foreign body capsule in an *ex ova* CAM wound healing model. Future work will quantify this biosensor data permitting further comparison to the physiological response. We are also transforming the *in vivo* model from the *ex ova* CAM to a small rodent mammal model.

The development of a novel type of biosensor providing a tool for assessing the biocompatibility of various coatings and surface treatments may stem from this work. Problems common to many *in vivo* sensors could be addressed with this versatile new tool.

ACKNOWLEDGMENT

The authors would like to thank the Washington Technology Center (WTC) for use of their electron microscope. They would also like to thank the members of the University of Washington MEMS lab for their technical assistance with instrumentation.

REFERENCES

- [1] E. T. McAdams and J. Jossinet, "Tissue impedance: A historical overview," *Physiol. Meas.*, vol. 16, pp. A1–A13, 1995.
- [2] H. P. Schwan, "Electrical properties of tissue and cell suspensions," in *Advances in Biological and Medical Physics*, J. H. Lawrence and C. A. Tobias, Eds. New York: Academic, 1957, vol. 5.
- [3] H. P. Schwan, "Determination of biological impedances," in *Physical Techniques in Biological Research*, W. L. Nastuk, Ed. New York: Academic, 1963, vol. 6.
- [4] S. Grimnes and O. G. Martinsen, *Bioimpedance and Bioelectricity*. San Diego, CA: Academic, 2000.
- [5] J. G. Webster, *Electrical Impedance Tomography*. New York: Adam Hilger, 1990.

- [6] W. S. Tait, *An Introduction to Electrochemical Corrosion Testing for Practicing Engineers and Scientists*. Racine, WI: PairODocs, 1994.
- [7] J. R. McDonald and E. Barsoukov, *Impedance Spectroscopy*, 2nd ed. Hoboken, NJ: Wiley, 2005.
- [8] Hetke and Anderson, "Silicon electrodes for extracellular recordings," in *Handbook of Neuroprosthetic Methods*. Boca Raton, FL: CRC, 2003.
- [9] D. Q. Ho, Y. M. Bello, G. L. Grove, J. Manzoor, A. P. Lopez, C. R. Zerweck, E. A. Pierce, J. L. Werkeiser, and T. J. Phillips, "A pilot study of noninvasive methods to assess healed acute and chronic wounds," *Dermatol. Surg.*, vol. 26, pp. 42–49, Jan. 2000.
- [10] N. Alikacem, Y. Marois, Z. Zhang, J. B. Jakubiec, R. Roy, M. W. King, and R. Guidoin, "Tissue reactions to polypyrrole-coated polyesters: A magnetic resonance relaxometry study," *Artificial Organs*, vol. 23, no. 10, pp. 910–919, Oct. 1999.
- [11] Y. Y. Duan, G. M. Clark, and R. S. C. Cowan, "Factors determining and limiting the impedance behavior of implanted bio-electrodes," in *Proc. SPIE*, 2001, vol. 4235, p. 498.
- [12] W. M. Grill and J. T. Mortimer, "Electrical properties of implant encapsulation tissue," *Ann. Biomed. Eng.*, vol. 22, no. 1, pp. 23–33, 1994.



Floyd B. Karp received the B.S. degree in metallurgy and materials science from Carnegie-Mellon University, Pittsburgh, PA, in 1978, and the M.S. degree in ceramic engineering, the Masters of Medical Engineering degree in 1981 and 2002, and expects the Ph.D. degree in bioengineering from the University of Washington, Seattle, in 2008.

Since 1981, he has worked in industry as a Materials Engineer contributing to the design and development of medical devices. He undertook a mid-career sabbatical in 2003 to pursue studies leading to

the Ph.D. degree.



Neil A. Bernotski (M'05) received the M.S. degree in electrical engineering from the University of Washington, Seattle, in 2002. He is currently working toward the Ph.D. degree at the same university.



Thelma I. Valdes received the B.B.E. degree from the Catholic University of America, Washington, DC, in 1997, and the Ph.D. degree in bioengineering from the University of Connecticut, Farmington, in 2006.

From 2004 to 2006, she was a Visiting Scholar in the Department of Bioengineering, University of Washington, Seattle. She now works as a Senior Research Scientist for Becton Dickinson and Company, Franklin Lakes, NJ.



Karl F. Böhlinger (SM'06) received the Diplom-Informatiker degree from the University of Karlsruhe, Germany, and both the M.S. and Ph.D. degrees in computer science from Cornell University, Ithaca, NY.

He spent a year as a Visiting Scholar at the Stanford University Robotics Lab and Transducer Lab. From 1996 to 1998, he was a Postdoctoral Researcher at the University of California, Berkeley. He is Professor of electrical engineering with adjunct appointments in computer science and engineering and in mechanical

engineering at the University of Washington, Seattle.



Buddy D. Ratner received the B.S. degree in chemistry at Brooklyn College, Brooklyn, NY, in 1967, and the Ph.D. degree in polymer chemistry from the Polytechnic Institute of Brooklyn, New York, in 1972.

He is a Professor of bioengineering and chemical engineering and Director of the University of Washington Engineered Biomaterials (UWEB), Seattle.